ACS APPLIED POLYMER MATERIALS

pubs.acs.org/acsapm Article

Melt-Fabricated Photoreactive Block Copolymer Micelles as Building Blocks for Tunable Elastomeric Hydrogels

Nabila A. Huq, René P. M. Lafleur, and Travis S. Bailey*

Cite This: *ACS Appl. Polym. Mater.* 2020, 2, 5377−5387 Read Online

ACCESS | Metrics & More | Article Recommendations | Supporting Information

ABSTRACT: Soft, conformally shaped thermoplastic elastomer (TPE) hydrogels producible from a moldable precursor material are desirable in many biomedical, surgical, and pharmaceutical applications. An innovative class of hydrogel networks was developed by employing photocurable, moldable solutions of melt-assembled spherical micelles formed from ω-anthracenyl-polystyrene-*b*-poly(ethylene oxide) diblock copolymer. Photo-induced [4 + 4] cycloaddition (λ = 365 nm) of terminal anthracene groups populating the hydrophilic corona of each micelle was used to produce polystyrene-*b*-poly(ethylene oxide)-*b*-polystyrene triblock copolymer tethers or network strands among adjacent micelles. Structural uniformity in the micelle population was confirmed by small-angle X-ray scattering (SAXS), cryogenic transmission electron microscopy (cryo-TEM), and dynamic light scattering (DLS). Homogeneous dispersal of the assembled micelle building blocks in water resulted in spreadable or moldable photoactive micelle solutions, studied for their stability in solution and ability to rapidly form elastomeric hydrogels once irradiated. Once in molds, these solutions of varied concentration were irradiated to form soft TPE hydrogels with dynamic shear modulus controllable with irradiation time (triblock copolymer content), exhibiting prescribed shape consistent with high-fidelity conformal fill.

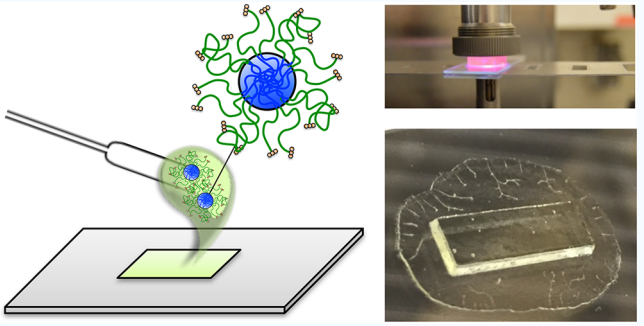

KEYWORDS: *hydrogel, thermoplastic elastomer, photocycloaddition, micelle, block copolymer, anthracene, physically cross-linked networks*

INTRODUCTION

Polymeric hydrogels are used in a large range of applications including separation membranes,[1,2] pharmaceuticals,[3−6] biomedical materials,[7−11] cosmetics, and personal hygiene products.[6,12,13] The efficacy of any particular hydrogel system does, however, require its properties be tailorable to the performance demands of the intended application. Factors such as mechanical behavior, malleability, chemical functionality, or biocompatibility, for example, must often be taken into account. Here, we disclose a versatile hydrogel system based on melt-fabricated photoreactive block copolymer micelle precursor solutions which exhibit an ability to be easily molded into specific shapes and subsequently photocured to create soft, yet elastomeric solids. Such materials have implications in facets of the above-mentioned application areas where an ability to generate a flexible hydrogel conformally shaped to the surrounding features is extremely desirable.[13,14] In particular, this two-component, photoreactive system distinguishes itself from others in its simplicity as well as its divorce of the self-assembly process from a photoreactive curing step that fixes the system without sacrificing the intrinsic thermoplasticity of the hydrogel. In addition, the moduli achievable are higher than other structurally similar systems, particularly those in which micelle self-assembly is accomplished in solution (not the melt).[15]

Our group has been exploring the practical use of sphere-forming block copolymer (BCP) morphologies as a foundation for a new class of thermoplastic elastomer (TPE) hydrogels.[16−20] These morphologies are generated by blending AB diblock and ABA triblock copolymers of a defined A-block volume fraction[21] chosen to drive formation of a periodic network of spherical micellar-shaped aggregates. The A and B blocks are selected such that the core (A blocks) of the spherical aggregate is intrinsically hydrophobic and glassy, while the corona (B blocks) is water-soluble. In these systems, the role of the ABA triblock copolymer is to bridge or tether adjacent spherical micelles. Much of this work has focused on the use of ABA triblock copolymer concentration as a dial through which the hydrogel mechanical properties can be tuned, with considerable effort spent on achieving high-

Received: February 4, 2020
Accepted: September 25, 2020
Published: September 25, 2020

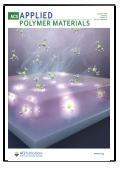

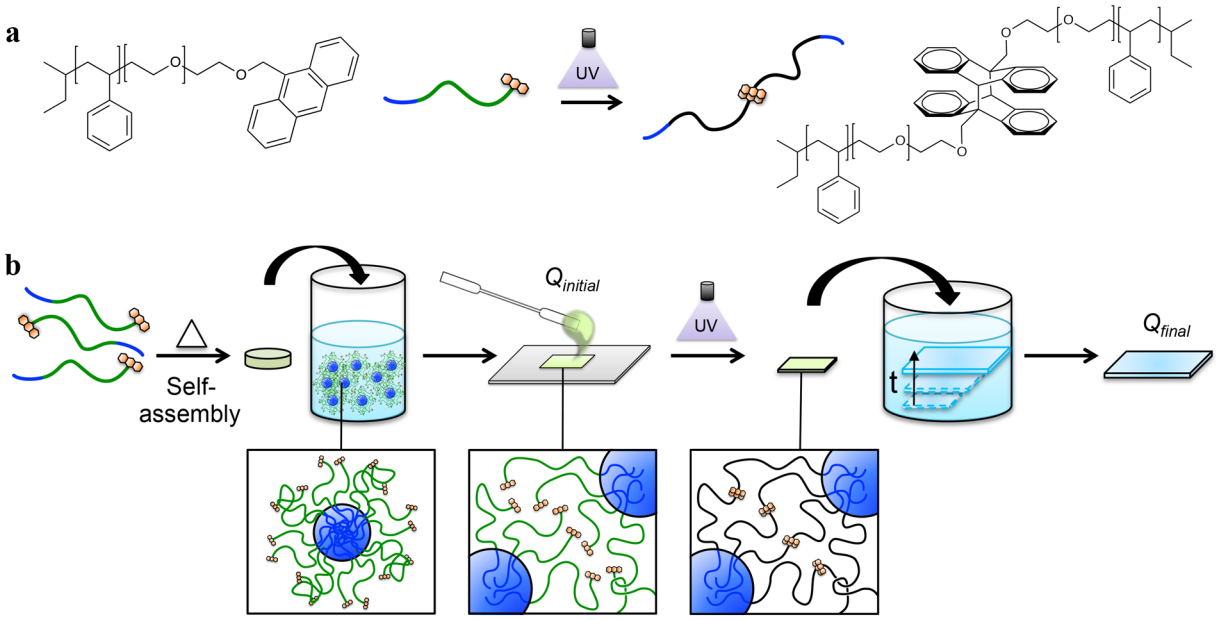

Figure 1. (a) Anthracene-functional SO (SO-anth) can be photocoupled to form SOS *in situ* using UV light. (b) SO-anth is self-assembled in the melt to form photoactive micelles composed of glassy PS cores and hydrophilic PEO coronas. These untethered micellar building blocks are dispersed in water (before any UV irradiation) to form viscous solutions of known weight ratios of water to polymer ($Q_{initial}$). These solutions can then be poured or smeared into a mold and UV-irradiated to form SOS triblock copolymer tethers *in situ*, producing the network architecture. The resulting hydrogel network, which is at the same $Q_{initial}$ as before solution molding and irradiation, retains the shape it was cured in. It is then placed in excess water and allowed to swell to its equilibrium dimensions characterized by Q_{final}, retaining its original (but enlarged) shape. Some components of this figure have been reproduced from ref 19.

modulus, fatigue-resistant systems formed entirely in the melt state.[22−24] However, by requiring the introduction of ABA triblock copolymer tethers during melt-state self-assembly, the shape in these systems must be set during thermal processing (100−200 °C). This limits direct incorporation of thermally sensitive additives (e.g., pharmaceuticals, living cells, etc.) and precludes use in point-of-care applications in which ambient temperatures and conformal shaping prior to gelation are advantageous.[25,26]

This work adapts our original TPE hydrogel system to one in which the basic micellar building blocks can now be dispersed into moldable solutions prior to network formation at ambient temperatures. The key challenge was to develop a system that would allow the thermal processing step required for micelle formation to be divorced from network formation. Our solution to this challenge is based on the replacement of the original AB/ABA BCP blend with a single-component AB diblock copolymer end-modified with a photodimerizable substituent (Figure 1a). This strategy permits the untethered micelles formed during melt processing to be easily dispersed in solution, prior to light-triggered chain coupling between micelles to induce network formation. This, in turn, allows us to maintain the efficient tethered-micelle network architecture of the original blended system while using only a single photoactive BCP species. The model system chosen to validate this new approach was a polystyrene-*b*-poly(ethylene oxide) (SO) diblock copolymer end-modified with anthracene (SO-anth). With intrinsically high water content and a majority of the hydrogel comprising micelle coronas made of biobenign PEO, such hydrogels offer the benefit of significant immunogenicity and biocompatibility;[27] such biocompatibility has been leveraged in a wide variety of applications.[28−30] The SO-anth BCP volume fraction was specifically synthesized to produce micellar building blocks containing a glassy polystyrene core with water-soluble poly(ethylene oxide) coronal layers.[21,31−33] When solutions of these micelles are UV-irradiated (λ = 365 nm), the SO-anth comprising the micelles couples to form symmetric polystyrene-*b*-poly(ethylene oxide)-*b*-polystyrene (SOS) triblock copolymer tethers *in situ*. This process occurs through a [4 + 4] photocycloaddition reaction between terminal anthracene substituents on the SO-anth. Such photocoupling of polymer chains through terminal anthracene structures has been shown to be reasonably efficient in our and other's previous work, achieving coupling efficiencies exceeding 80% in the melt even for chain molecular weights approaching 100 kDa. While such efficiency is reduced to 30−40% in the more dilute systems studied here (as a result of both a reduced concentration of anthracene end-groups and their potential to selectively segregate into the PS/PEO interfacial region or PS cores), these levels are much greater the observed minimum threshold required for gelation (<3%).[16,19,34]

The moldable or pourable micelle solutions were rapidly transformed with only minutes of UV exposure to soft, elastomeric hydrogels. The resulting solids preserved their shape once removed from their molds and maintained a low enough modulus to remain highly flexible. The experiments in this study examine how such attractive properties emerge by closely examining (1) the influence of integrated anthracene substituents on the micelle self-assembly process, (2) the stability of the dispersed micelles in solution over time, and (3) the effects of micelle concentration and UV irradiation time on the mechanical properties and swelling behavior of the hydrogel networks produced by using this approach (Figure 1b).

https://dx.doi.org/10.1021/acsapm.0c00108
ACS Appl. Polym. Mater. 2020, 2, 5377−5387

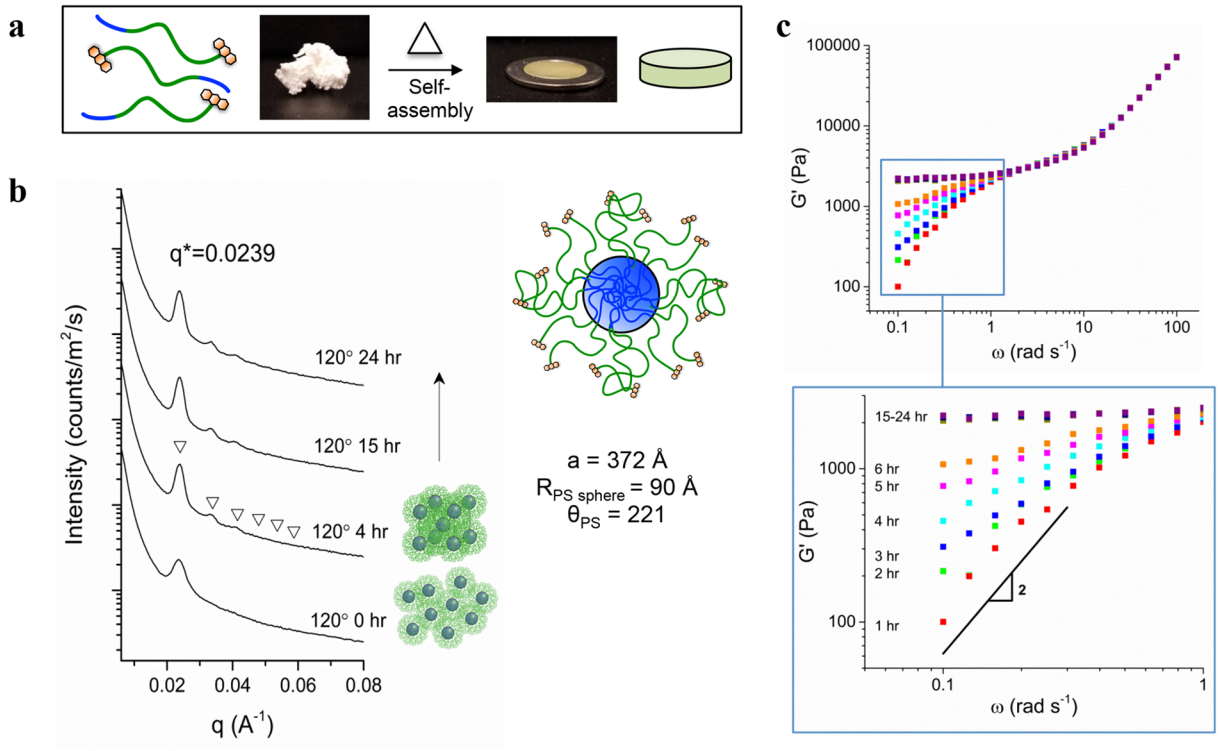

Figure 2. (a) SO-anth was pressed from a white powder into yellow-tinged translucent disks by heating to melt-state, inducing self-assembly into a periodic morphology of nanoscale micellar domains. The morphology and size of the micelles as a function of annealing time at 120 °C were investigated by using (b) SAXS and (c) rheological frequency sweeps. Adoption of a BCC lattice appears to occur only after annealing of the samples for about 4 h, with continued evolution of the morphology beyond 4 h suggested by eventual formation of a plateau in the rheological data.

RESULTS AND DISCUSSION

Synthesis and Structure SO-anth Micellar Building Blocks. The synthesis of the SO-OH diblock copolymer (f_{PS} = 0.122, M_n = 73800 g mol^{-1}, PDI = 1.04) parent to the SO-anth diblock copolymer was performed by using anionic polymerization techniques.[16] End-functionalization of the SO-OH with anthracene was accomplished through displacement of the chlorine on 9-chloromethylanthracene by nucleophilic substitution using the potassium alkoxide of the terminal hydroxyl end-group of SO-OH.[35] Functionalization was estimated to be approximately quantitative by using ^{1}H NMR peak integrations (Figure S1). The molecular weight distribution of the SO-anth product was confirmed by using size exclusion chromatography (SEC) and resembled that of the parent SO-OH, indicating no evidence of chain degradation. Importantly, measures were taken to reduce inadvertent light exposure during SEC sample preparation (see the Experimental Section) to avoid premature chain coupling.

The SO-anth diblock copolymer product was then used as the sole polymeric component in this solution-based pourable hydrogel fabrication method, effectively comprising three steps as follows, and is described in further detail in the Experimental Section. First, the block copolymer was self-assembled in the melt to form spherical micellar structures (120 °C, 5 min), containing a hydrophobic polystyrene core and a poly(ethylene oxide)−anthracene corona. Next, these photoactive micelles were combined with water in specific ratios ($Q_{initial}$ = 8, 12, 16, and 20 g of water per g of polymer) to form solutions of varying viscosity and micelle concentration (and thus mean intermicelle spacing). Finally, these micelle solutions were poured or smeared (depending on solution viscosity) into molds and photocoupled by using UV light (λ = 365 nm, I = ∼30 mW cm^{-2}). This exposure induced dimerization of the terminal anthracene substituents, creating SOS triblock copolymer tethers (network strands) between micellar building blocks. The resulting soft thermoplastic elastomer hydrogels produced from this three-step process were then placed in water and allowed to swell to their final equilibrium dimensions.

The BCP volume fraction (f_{PS} = 0.122, M_n = 73800 g mol^{-1}) was selected such that phase separation in the melt produces spherical micelles, which for the PS−PEO block copolymer systems has been found to form in the f_{PS} = 0.07−0.13 range.[16,17,19,31,36] Phase separation at such volume fractions can produce spherical micelles quite rapidly, but development of highly ordered lattices such as the thermodynamically preferred body-centered-cubic (BCC) morphology can often require extended annealing.[36−39] Such annealing is necessary to overcome kinetic barriers related to chain entanglements or slow chain dynamics, which constrains early ordering to a liquid-like packing (LLP) of micelles,[16,18,19,36] even at moderate molecular weights.[36−39] Because of our intention to use these micelles as the fundamental building blocks comprising the final hydrogel network, it was critical to understand the role of the emergent BCC structure in the melt as an indicator of eventual micelle structural integrity and size distribution uniformity once in solution. SO-anth BCP pressed from a white powder into yellow-tinged, translucent disks was subjected to various tests to further probe properties of these building blocks (Figure 2a).

https://dx.doi.org/10.1021/acsapm.0c00108
ACS Appl. Polym. Mater. 2020, 2, 5377−5387

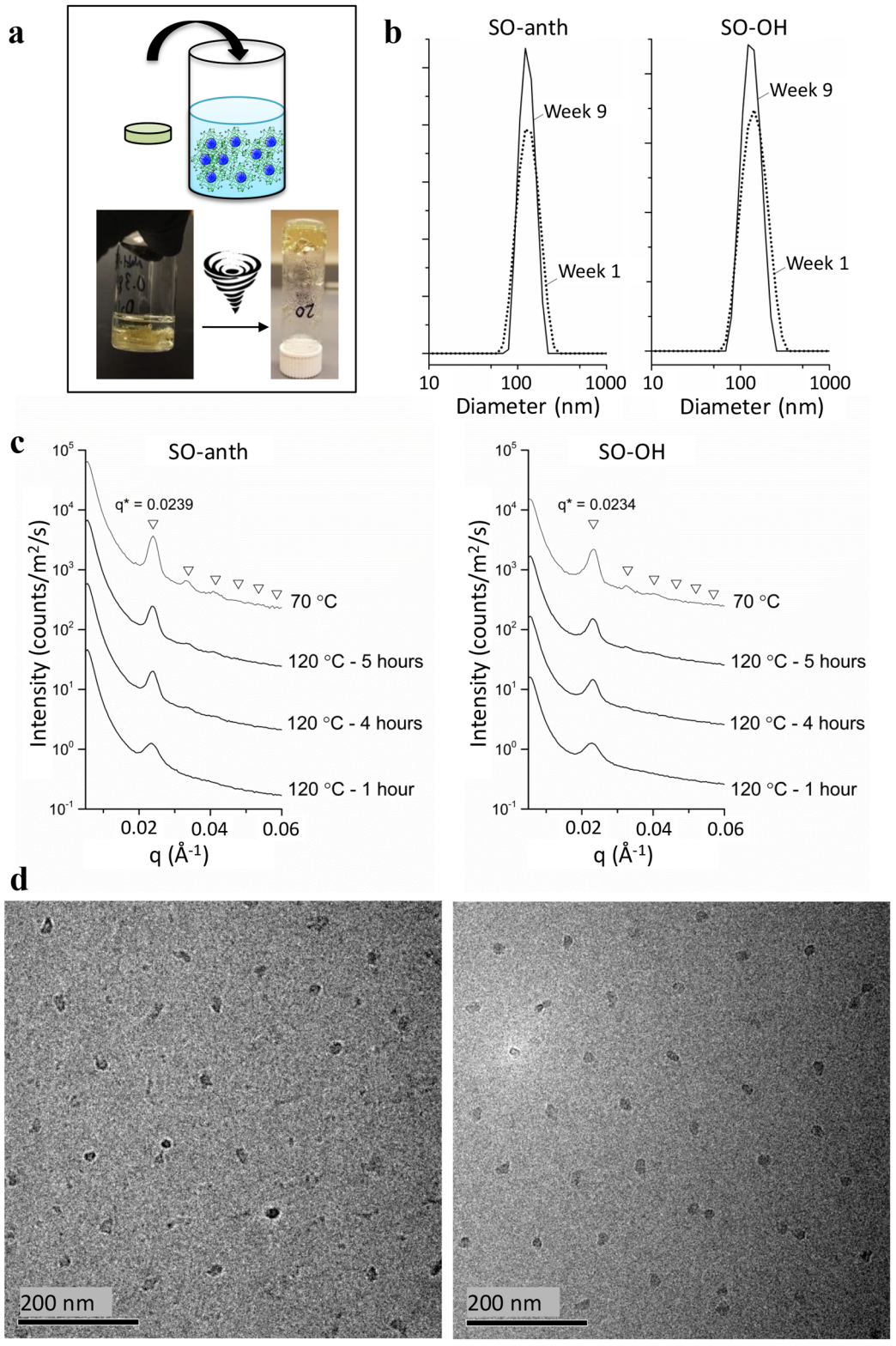

Figure 3. (a) Self-assembled micelles were combined with water and then vortexed to form a viscous, yellow-tinged solution. (b) Micelle stability and behavior in water was monitored over 9 weeks by using DLS, during which there was no evidence of aggregation. (c) SAXS data confirmed the emergence of BCC morphology after 4 h of annealing at 120 °C, with persistence of this organization upon cooling to 70 °C, prior to quenching. (d) Cryo-TEM images of micelles produced after quenching melt blends from 70 °C followed by dispersion of micelles in water (SO-anth: left; SO-OH: right). Images showed evenly spaced micelles with identifiable nonspherical PS cores. Hydrated PEO coronas appear indistinguishable from the surrounding solution.

The transition from LLP to BCC in SO-anth was suspected to occur between 110 and 140 °C from a series of rheological temperature ramp measurements in which a clear increase in elastic modulus was producible with extended annealing

https://dx.doi.org/10.1021/acsapm.0c00108
ACS Appl. Polym. Mater. 2020, 2, 5377−5387

(Figure S2). To investigate this supposition, small-angle X-ray scattering (SAXS) data were collected on samples during annealing at 120 °C (following cooling from the disordered state). Evolution of the initially formed LLP phase to a BCC lattice was detected via the emergence of a clear diffraction pattern in the SAXS data after 3−4 h (Figure 2b) of annealing time. A comparison of this self-assembly behavior to that of its SO-OH precursor (Figure S3) shows that while SO-OH seems to adopt a BCC structure slightly faster than SO-anth, the SO-anth diffraction pattern was ultimately more defined. Such subtle differences in phase behavior as a result of differences in chain-end functionality have been previously documented.[40] The presence of the terminal anthracene functional groups seemed to also have a minor impact on the lattice constants ($a_{SO\text{-}anth}$ = 37.2 nm vs a_{SO} = 37.8 nm) and chain aggregation numbers ($\theta_{SO\text{-}anth}$ = 221 vs θ_{SO} = 232) produced in the final morphologies (Table S1). With such small differences, it is difficult to ascertain the role in which interactions among anthracene units or between anthracene units and polystyrene domains are determining the subtle differences in morphological characteristics.

The evolution of the BCC morphology developed in SO-anth was probed by using a rheological frequency sweep under oscillatory shear at 120 °C (ω = 1 rad s^{-1}, γ = 7%). At early annealing times, the morphological structure produced still exhibits terminal relaxation behavior consistent with liquid-like behavior of the micellar units. As annealing proceeds, this slope in log G' vs log ω begins to evolve from its initial terminal value near two and slowly approaches zero (Figure 2c). This is consistent with the transition observed in the SAXS data, from a state with significant structural disorder to that of a highly developed BCC lattice.[41] The rheology data indicate that the sample reaches its final plateau modulus after ∼15 h, after which no significant changes are apparent. Interestingly, there is no clear difference between the BCC diffraction pattern adopted after 4 h of annealing and those recorded at the 15 or 24 h time points (Figure 2b). This difference indicates either that the rheological measurements are more sensitive to the evolving correlation among spheres of the BCC morphology than the SAXS measurements obtained by using our laboratory-scale instrument or that the dynamic oscillatory shear is necessary to accelerate the morphological evolution. Support for the latter may come from several studies in which dynamic shear was actually used to accelerate morphological development.[42−44] As before, a comparison of this rheological behavior to that of the SO−OH precursor (Figure S4) shows the evolution of the BCC structure occurs similarly, although slightly faster than SO-anth with terminal behavior indicative of less disorder at early annealing times.

Precure Micelle Solution Behavior. To form solutions of free micelles, disks of vitrified self-assembled SO-anth spheres were added to argon degassed DI water in specific ratios, quantified as $Q_{initial}$ (g of water per g of polymer). This slightly modified definition for Q was selected to facilitate comparisons in water content changes throughout preparation, UV exposure, and subsequent swelling throughout this work. The micelles were allowed to passively disperse over 24−48 h before being briefly vortexed to ensure even distribution and dissolution. The resulting homogeneous mixtures were then given time to consolidate into clear viscous solutions, possessing a yellow tint associated with the anthracene substituents (Figure 3a). Even though BCC organization is achieved only after prolonged annealing as seen in Figure 2, DLS data on solutions containing micelles at various extents of annealing showed no significant difference in hydrated micelle size distribution (Figure S5). This result suggests that the absence of the BCC morphology during melt assembly has no consequence with respect to micelle size inhomogeneity in solution on a level detectable by DLS and that the 5 min, 120 °C heat pressing step is sufficient to achieve uniformity in micelle size. This implies micelle fabrication times can be greatly reduced from those required to achieve BCC morphology, in that the extended annealing needed for BCC morphology development is unnecessary in terms of micelle uniformity, size, or structure once dispersed in solution. The ability to produce micelles of relative uniformity without long processing times is an attractive feature of these systems.

To assess micelle stability in water, solutions were analyzed over a period of 9 weeks. DLS was used to identify undesirable dissolution or aggregation of micelles, and SEC was used to detect potential BCP chain degradation. DLS data showed consistency in the SO-anth micelle size distribution over the 9 week period, with no evidence of dissolution or aggregation (Figure 3b). The only discernible difference in DLS data between weeks one and nine was a slight narrowing in the size distribution seen in both SO-anth and SO-OH micelles. We believe that such narrowing in the calculated distribution is likely associated with the degree of chain entanglement between of the micelles becoming more uniform with time. This is reflected in more uniform hydrodynamic diffusive behavior, resulting in the narrowing of the measured size distribution. That is, this narrowing is not likely a product of actual changes in the number of chains per micelle aggregate. This would be consistent with the vitreous nature of the polystyrene cores, long-term shape preservation previously observed in our TPE hydrogel systems,[16−19,45] and the demonstrated nonergodicity of BCP micelles,[46] all of which suggest room temperature chain exchange among micelles is essentially nonexistent over this time scale. Additionally, SEC measurements confirmed the absence of chain degradation over the 9 week period, although a small amount (<5%) of photocoupling was detected by week nine (Figure S6). We suspect that the appearance of SOS in the SEC data is a result of inadvertent light exposure over the 9 week period and is essentially limited to intracoronal dimerization of SO-anth chains, as we did not observe micelle aggregation in the DLS data. The stability of the system was also apparent in the SO-OH precursor confirmed by using DLS (Figure 3b) and SEC (Figure S6) data.

Micelle dimensions and size uniformity were confirmed by using cryogenic transmission electron microscopy (cryo-TEM). Micelles were prepared by using two processing methods. The first was our preferred method of self-assembly without extended annealing. The second involved annealing at 120 °C in a SAXS instrument until BCC organization was confirmed, followed by quenching from 70 °C, just above the PEO crystallization temperature (Figure 3c). Quenching in this manner was done in an attempt to maximize retention of the morphological characteristics developed in the melt. Cryo-TEM images of micelles produced by either processing method contain dark regions consistent with dimensions of the PS cores expected from the SAXS data (∼18 nm diameter, Figure 3d). As expected, the highly hydrated PEO coronas cannot be distinguished from the background solution due to similarities in electron density. However, the regular spacing between the PS cores implies micelle dimensions (∼122 nm, core to core)

https://dx.doi.org/10.1021/acsapm.0c00108
ACS Appl. Polym. Mater. 2020, 2, 5377−5387

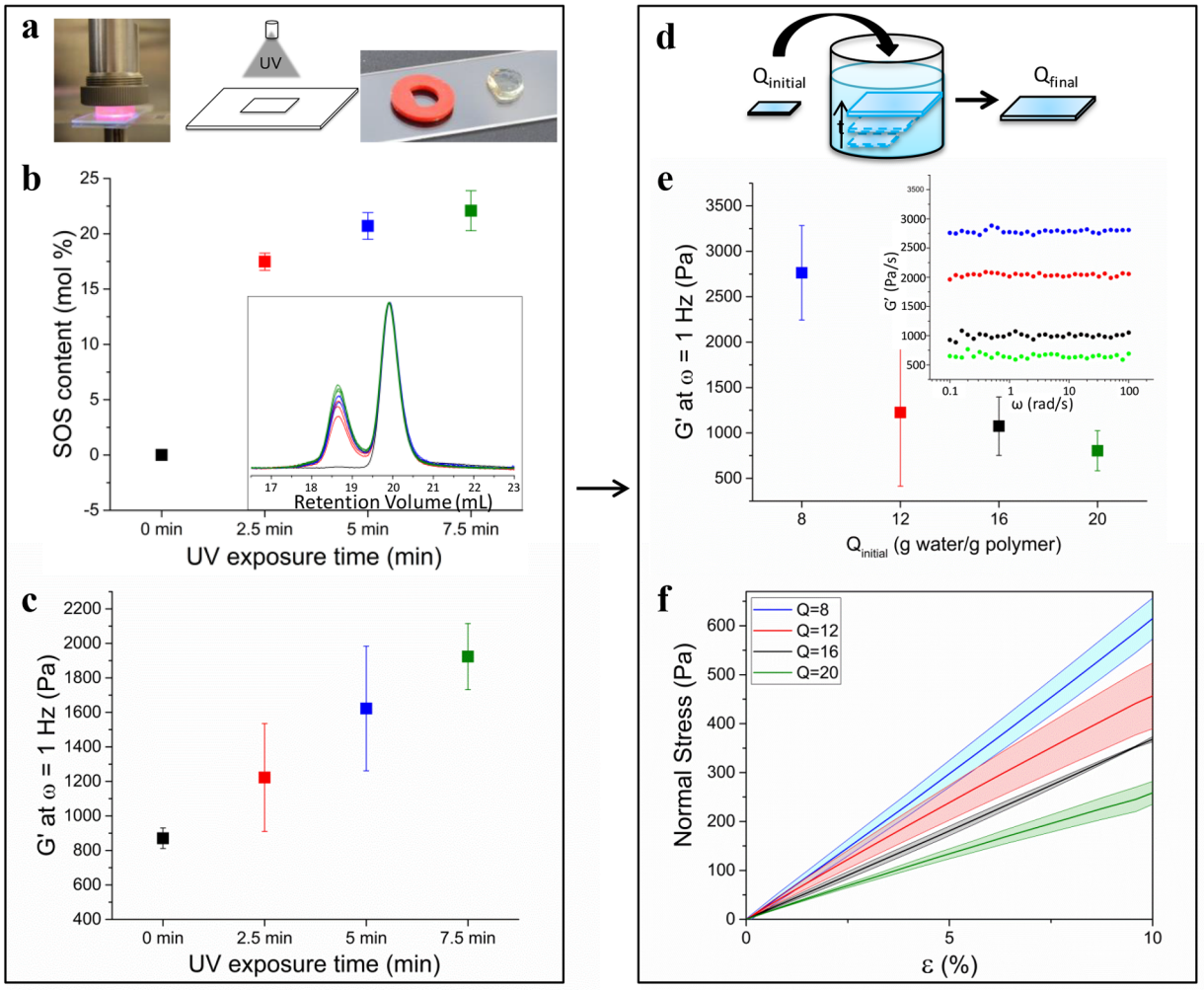

Figure 4. (a) $Q_{initial}$ = 16 g of water per g of polymer solutions was spread into molds and photocoupled by using UV light. (b) Installed triblock content based on SEC data was positively correlated to UV exposure time. (c) Shear elastic modulus at room temperature extracted from frequency sweeps (ω = 1 Hz, γ = 7%) was also positively correlated to irradiation time. (d) Samples of photocured hydrogels were then swelled to their equilibrium dimensions in DI water (Q_{final}). (e) Shear elastic modulus (ω = 1 Hz, γ = 7%) and (f) tensile modulus were negatively correlated to $Q_{initial}$ (2% s^{-1}). Mean and standard deviation shown for all data.

that are consistent with the hydrodynamic diameter suggested by the DLS data (~128 nm). Interestingly, both preparation methods yielded nonspherical PS cores. In theory, while the distortion in shape could be associated with random fluctuations in core domain shape in the melt that are trapped during vitrification, we suspect it is more likely a product of PS domains being unable to fully vitrify prior to PEO crystallization near 65 °C. That is, the domains experience strain-induced deformation[16,47] as a result of crystallite formation in the surrounding PEO matrix. This would be consistent with our previous DSC data, which suggests the PS T_g in the nanoscale domains may be depressed from its expected bulk value (~80 °C).[16] This would also explain the limited efficacy of our attempt to suppress the effects of crystallization and retain morphological characteristics of the developed BCC lattice through quenching from just above the PEO crystallization temperature.

UV-Triggered Hydrogel Formation. In this study, solutions with water to polymer mass ratios ($Q_{initial}$) between 8 and 20 g of water per g of polymer were spread into molds, sandwiched between hydrophobic glass slides, and exposed to UV light (λ = 365 nm, I ~ 30 mW cm^{-2}) for up to 7.5 min to form soft hydrogels (Figure 4a). These hydrogels were then be swollen to new equilibrium dimensions in argon-degassed water as a result of the system's thermodynamic requirement to balance the osmotic swelling forces against the entropic resistance to swelling provided by the newly formed tethers (Figure 4d). This new equilibrium ratio of water to polymer (termed Q_{final}) notably always exceeded $Q_{initial}$ for the system, a result of being able to swell beyond the minimal initial stress state of the tethers at the time of installation (at $Q_{initial}$).

To study the effect of irradiation time on SOS concentration and, ultimately, the hydrogel mechanical properties, solutions of $Q_{initial}$ = 16 g of water per g of polymer were placed in glass-sandwiched molds and exposed to UV light for a total of 2.5, 5, and 7.5 min. Molds were flipped over halfway through the targeted irradiation times to ensure equivalent exposure from top and bottom, providing axially symmetric tether installation. SEC data showed installed SOS content increased with increasing exposure time, with a majority of the SOS triblock copolymer formation occurring within the first 2.5 min (Figure 4b). We suspect that the rapid coupling is a consequence of a tendency for terminal anthracene units to preorganize through $\pi-\pi$ stacking[48] and hydrophobic interactions in water.

https://dx.doi.org/10.1021/acsapm.0c00108
ACS Appl. Polym. Mater. 2020, 2, 5377−5387

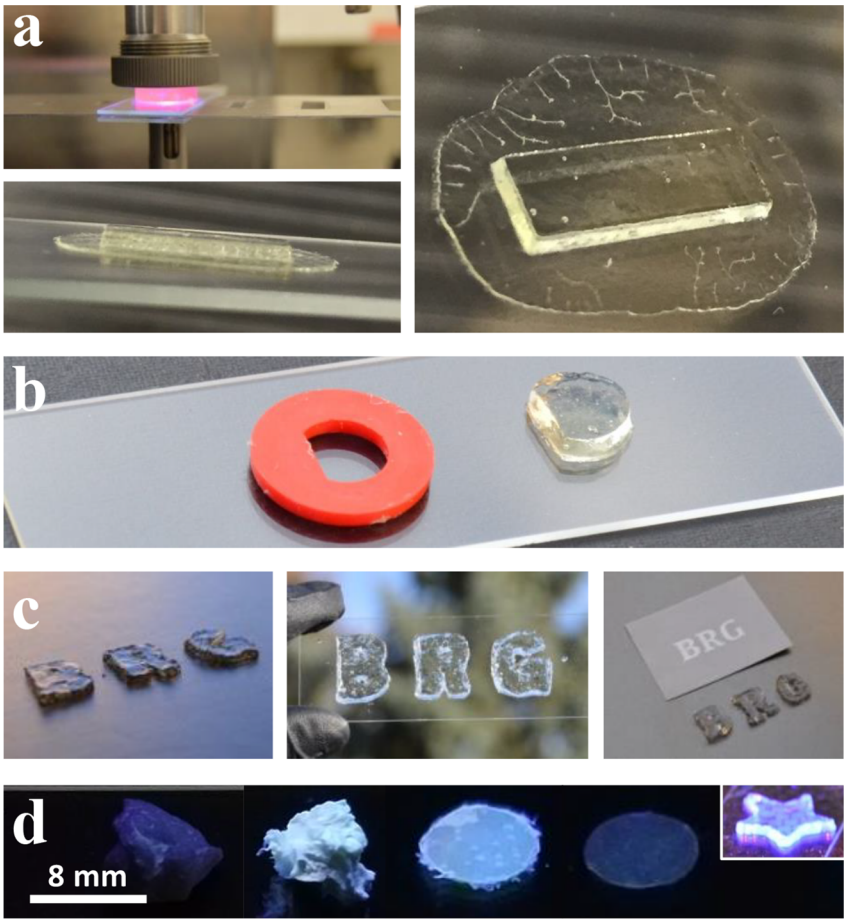

Figure 5. (a) Solutions can be molded and irradiated to form distinctly shaped, soft, elastic hydrogels. In the upper panel, $Q_{initial}$ = 20 g of water per g of polymer was spread into a thin rectangular cutout, previously fixed at the bottom edge to a glass slide (1 in. × 3 in. shown in panels a−c).

Notably, extended irradiation past this time did not appear to increase the SOS content to a great extent. This is thought to be a product of highly spaced photoactive micelles in these dilute systems as well as intrinsic local constraint of chain ends anchored in the micelle core. After swelling the photocoupled samples to equilibrium (Q_{final}), dynamic frequency sweep data (ω = 0.1−100 rad s^{-1}) displayed plateau behavior (frequency independence) in the elastic moduli, typical of elastic solids.[41] The mean elastic modulus extracted from each of these sweeps was positively correlated to UV exposure time, indicating increased modulus with increasing triblock copolymer content (Figure 4c). Our previous studies on melt systems suggest this increase in modulus is not only due to the increase in network strands (tethers) in the system but also the result of increased overlap between coronal domains at Q_{final}. This increased overlap is a result of restricted swelling imposed by entanglements trapped among the strands during photocoupling.[17] In a proof-of-concept study immediately preceding this work, we investigated the photocoupling potential of SOanth in the dry melt state where the concentration of chain ends is maximized.[19] Equilibrium-state hydrogels formed from these initial studies through melt photocoupling exhibited moduli in the range of G' = 1−100 kPa. In contrast, the elastic shear modulus values of hydrogels made as a result of photocoupling $Q_{initial}$ = 16 solutions (G' = 0.6−2.1 kPa) were significantly lower. We suspected that the reduced moduli produced during solution coupling were a direct consequence of fewer entanglements among the tethering chains (strands) during UV irradiation, in contrast to their melt-photocoupled counterparts. This observation suggested a high potential to tailor the modulus of the resultant hydrogels through adjustment of micelle concentration. That is, changing the water-to-polymer ratio would directly influence the mean spacing between micelles, controlling the coronal overlap and entanglement density at the time of photocoupling. Additionally, the decreased micelle proximity relative to the melt-photocoupled system increases the probability of intramicelle photodimerization, resulting in a fraction of the SOS triblock copolymer formed having PS end blocks that occupy the same micelle core. These looping SOS chains, while not distinguishable from tethering SOS chains experimentally, still contribute to the measured SOS content by using SEC. However, looping SOS chains are unlikely to contribute to the mechanical properties of the hydrogel network, further emphasizing the influence of micelle concentration during hydrogel formation.

To test this theory, solutions of $Q_{initial}$ = 8, 12, 16, and 20 g of water per g of polymer were spread into glass-sandwiched molds and then exposed to UV light for 5 min before swelling to Q_{final}. Interestingly, the values of Q_{final} were only moderately influenced by $Q_{initial}$ solution concentrations, each appearing to approach a mean final value between 18 and 21 g of water per g of polymer (Figure S7). In fact, the difference between Q_{final} and $Q_{initial}$ appears to diminish with increasing $Q_{initial}$, with minimal additional swelling occurring after photocoupling at $Q_{initial}$ = 20. Hydrated micelle dimensions estimated using cryo-TEM images show consistent core-to-core distances in the 120

https://dx.doi.org/10.1021/acsapm.0c00108
ACS Appl. Polym. Mater. 2020, 2, 5377−5387

nm range, which roughly corresponds to Q values near 30 g of water per g of polymer, based on estimates of volume occupied per hydrated micelle. Assuming the close micelle packing observed in the images is representative of the length scale at which the coronal chains of the micelles just begin to interact, tethers formed at $Q_{initial}$ = 20 occur at a point of minimal coronal overlap (~5 nm). Thus, at dilute $Q_{initial}$ values, the tethers formed are already quite extended. In contrast, at $Q_{initial}$ = 8 where the overlap is much more substantial, the tethered micelle network formed has a larger capacity to swell. However, increased entanglements accompanying this overlap simultaneously serve to counter this swelling, such that Q_{final} values remain smaller than those associated with more dilute systems.

To assess the correlation between mean intermicelle spacing (implied by $Q_{initial}$) and mechanical characteristics of the resultant hydrogels at Q_{final}, each equilibrium swollen sample was subjected to rheological and tensile testing. Dynamic frequency sweeps confirmed a frequency-independent elastic modulus in all hydrogels (Figure 4e, inset) in the series, with the mean value of the elastic moduli taken at ω = 1 rad s^{-1} being negatively correlated to increasing $Q_{initial}$ (Figure 4e). That is, the more water per gram of polymer in the system at the time of photocoupling ($Q_{initial}$), the lower the modulus of the hydrogel in its final swollen state (Q_{final}). Given the minimal influence of $Q_{initial}$ on the final SOS content (Figure S8), it appears the decrease in modulus is likely related to the decrease in the bridging-to-looping ratios present in each of these systems as a consequence of the change in micelle spacing. Additionally, the increased distance between micelles may also increase the opportunity for anthracene end-groups to bury closer to the hydrophobic micelle core, though experiments were not performed to ascertain the likelihood of this over intramicelle dimerization.

Finally, preliminary tensile testing revealed a positive correlation between small-strain tensile modulus and $Q_{initial}$ (Figure 4f). Past 10% strain, hydrogels were likely to slip from the tensile test fixture prior to failure due to their high lubricity and low modulus. Although preliminary, this data confirmed the trend demonstrated by the oscillatory shear experiments discussed above, in that small strain tensile modulus is negatively correlated to $Q_{initial}$. Taken together, these results demonstrate the ability to fine-tune the final modulus simply by tailoring the amount of water used to disperse the micelle building blocks.

Patterning and Shape Control. The ability of these solutions to rapidly transform from viscous liquids to physically cross-linked but soft, highly entangled, low-modulus hydrogels makes them ideally suited for applications that require high surface area conformal contact, flexibility, and rapid adoption of well-defined macroscopic shapes when molded (Figure 5a,b). These photographs show the ability of the photocoupled hydrogel to hold a precise edge even after removal from the mold. Network formation through UV irradiation also implies an intrinsic ability for the introduction of shape through photopatterning. In theory, masked regions can be easily removed due to the absence of tethers (network formation) among micelles in those areas. As shown in Figure 5c, simple letter shapes were patterned into spread solutions and extracted after rinsing, although edge roughness associated with the scattering of UV light from small gas bubbles is clearly evident. A true assessment of the patterning precision possible in these systems will require removal of bubble inclusions from the solutions prior to UV irradiation. The fluorescence of anthracene and the absence of this fluorescence in the photocycloaddition product allow us to visualize the regions in which photodimerization among SO-anth has occurred to produce the micelle network.[49,50]

The left side of Figure 5d depicts powder of SO-OH juxtaposed with powder of SO-anth, showing the strong fluorescence produced even at anthracene concentrations equivalent to one substituent per polymer chain. To the right of this is a self-assembled, pressed disk of SO-anth showing the same fluorescent behavior, followed by an irradiated analogue for which dimerization has been maximized through photocoupling in the melt. A comparison of the two disks shows the clear loss of fluorescence upon significant photodimerization of the SO-anth, such that its appearance is similar to the background luminescence associated the nonanthracene functional SO-OH powder. In contrast to coupling in the melt, solution photocoupled systems continue to fluoresce (photopatterned star, inset) even after extended exposure. This residual fluorescence is thought to be a consequence of unreacted anthracene substituents that have been effectively isolated. Such isolation, we suspect, is a combination of early infinite network formation at very low thresholds of anthracene dimerization (~2%), which limits future micelle interactions, in combination with chain anchoring to fixed positions in the micelle core, which limits local chain end mobility. As irradiation proceeds, a fraction of the chain ends become unable to find a dimerization partner in their accessible reaction volume. Other possible sources of limited triblock copolymer formation may derive from nonquantitative functionality present in the initial SO-anth materials, kinetic restrictions on micelle and chain mobility due to high molecular weight entanglements, or the inaccessibility of anthracene-functional chain ends due to being trapped deep within the coronal layer or even the glassy micelle core itself.

The spread solution was then compacted by using a second glass slide, allowing excess material to spread outside the perimeter of the mold's upper face. Extraction from the mold shows the level of conformal integrity achievable by the photocoupled sample throughout the entire depth of the mold. (b) Example of a hydrogel formed in a mold (1.73 mm thickness) at $Q_{initial}$ = 20 g of water per g of polymer, subsequently swollen to Q_{final} following extraction and removal of all peripherally photocoupled (excess) material. (c) Shape was also be imposed through photopatterning by using masks to spatially control the introduction of SOS tethers, however, with some surface roughness associated with scattering of UV light from small gas bubble inclusions. (d) Left to right: SO-OH powder, SO-anth powder, disk of self-assembled SO-anth micelles, and photocoupled SO-anth micelles. Irradiated SO-anth looks akin to SO-OH, consistent with the expected loss of fluorescence upon photocycloaddition to form the dimer. Inset: a star-shaped hydrogel (produced using a star-shaped mask) retains some fluorescence (in contrast to melt photocoupled samples) due to residual orphaned anthracene end-groups, present even after longer exposure times.

CONCLUSIONS

Photoreactive block copolymer micelles formed through self-assembly of SO-anth in the melt were dispersed in water to form spreadable precursor solutions easily transformed into soft, elastic hydrogels with UV irradiation. Rapid preparation of these micellar building blocks was achieved by using BCP

https://dx.doi.org/10.1021/acsapm.0c00108
ACS Appl. Polym. Mater. 2020, 2, 5377−5387

compositions favoring adoption of the sphere morphology. Micelle structure created during initial phase separation (~5 min) was sufficient to produce narrow size distributions and shape uniformity, such that evolution of the morphology to the full BCC structure through extended annealing (>4 h) was not required. Micelles were stable in water without evidence of aggregation or degradation over a period of at least 9 weeks. Equilibrium swelling (Q_{final}), dynamic elastic modulus, and tensile modulus were tunable by using both UV irradiation time and initial micelle concentration ($Q_{initial}$). UV irradiation time at constant $Q_{initial}$ was positively correlated to SOS concentration, resulting in increased dynamic elastic modulus. Conversely, decreasing $Q_{initial}$ (micelle spacing) under constant irradiation time was used to produce higher moduli and limit Q_{final}. Photocoupling in molds was used to generate custom shapes with excellent conformal integrity and retention of form upon swelling. Preliminary experiments suggest the potential to also introduce shape through photopatterning. Overall, the ability to selectively disperse these micelle building blocks into stable, moldable solutions allows us to produce soft, flexible, conformable hydrogels without the presence of harmful solvents or other leechable small-molecule byproducts, sometimes seen in other soft hydrogel production strategies.[14] We anticipate these desirable attributes will have implications in a number of biomedically relevant applications including wound healing, surgical reconstruction, soft tissue repair or replacement, and cosmetics substances.

EXPERIMENTAL SECTION

Materials. *General.* The materials associated with the syntheses of SO, SOS, and SO-anth, their purification prior to use, and general handling procedures have been described previously.[19,26] Specific details associated with the use of these procedures in this work have been included in the Supporting Information.

Synthesis of PS−PEO (SO) and PS−PEO-Anthracene (SO-anth). Hydroxyl-terminal polystyrene-*b*-poly(ethylene oxide) (PS−PEO, SO)[16] and anthracene-terminal polystyrene-*b*-poly(ethylene oxide) (PS−PEO-anthracene, SO-anth)[19] were synthesized according to previously reported procedures.[16,19] These methods were employed for the synthesis of a hydroxyl-terminal polystyrene (PS) macroinitiator ($M_{n,PS}$ = 8064 g mol^{-1}, $M_{w,PS}/M_{n,PS}$ = 1.05, SEC (PS standards), from which the final SO and SO-anth diblock copolymers (overall M_n = 73800 g mol^{-1}, D = 1.04 (SEC, PS standards), f_{PS} = 0.122 (PS volume fraction calculated using nominal densities at 140 °C)[51]) were produced. The overall M_n was calculated by using the SEC measured $M_{n,PS}$ of the PS macroinitiator and the relative ^{1}H NMR integrations of the final SO and SO-anth diblock copolymers.

Recovered SO-anth was redissolved in THF with 0.5 wt % butylated hydroxytoluene (BHT) added to act as a radical scavenger. The polymer was then dried in vacuo (25 °C, ~24 h) to produce a final, yellow-tinged powder. The overall yield was 90%. SEC (D = 1.04 (PS standards)) confirmed no change in dispersity or molecular weight distribution following addition of anthracene to the chain terminus. Detailed ^{1}H NMR peak assignments can be found in the Supporting Information (Figure S1). Relative integrations of anthracenyl and initiator methyl protons suggest a quantitative addition of anthracene within ^{1}H NMR integration error (~5%).

Photoactive Sample Handling and Storage. Once functionalized with the photoreactive end-groups, polymers were handled to minimize light exposure. All samples were stored under argon in foil wrapped vials and kept in the dark. When removed from storage for subsequent processing, laboratory lighting was reduced as much as possible.

Synthesis of Micelle Solutions. SO-anth was pressed between Teflon sheets at 120 °C for 5 min by using any thin (<5 mm) mold to prevent spreading of the material during compression. For annealing studies, this pressed material was then further annealed at 120 °C either in nitrogen (using a rheometer) or in a vacuum (in the SAXS) for a range of times (up to 24 h in some SAXS experiments, as seen in Figure S3). Solutions of SO-anth polymer were pressed without annealing and combined in specific quantities with degassed DI water. These solutions are used throughout the study in varying concentrations depending on the application, and the relative amounts of water and polymer used are quantified by the value Q (g of water per g of polymer) which range from Q = 8 to 1000. Containing vials of just-made solutions are topped off with argon gas and left to sit for 24−72 h (depending on their Q) to allow the polymer to soften and mix with the water and subsequently vortexed for 10 s and allowed to settle. Solutions were used as soon as they appeared well-mixed with no visible solid suspensions. Solutions of equal concentration were subjected to identical dissolution procedure times for consistency between solution batches.

Hydrogel Formation. Molds were temporarily adhered to a hydrophobically treated (by using Rain-X) glass slide with double-sided tape. Sample solutions were then scooped into molds of varying shape, size, and material (see Figure 5 for examples; molds no thicker than 1 cm were used) by using a spatula and then sandwiched by using a second treated glass slide also adhered with the tape to prevent movement of the setup during irradiation and when turning over halfway through irradiation time. UV curing was induced via an OmniCure Series 2000 UV curing system (200 W Hg-arc lamp, Asahi Spectra Co., high-transmission 365 nm band-pass filter). Intensities at the surface of the sample were measured at 28−32 mW cm^{-2} (Omnicure R2000 radiometer). Samples were exposed to UV 365 nm filtered light for 2.5−7.5 min and flipped over halfway through the exposure time. The glass slide-sandwiched mold setup along with short exposure times and typical humidity of the laboratory environment allowed for a system that largely prevented water evaporation during UV exposure.

Measurements. *NMR, SEC, and SAXS.* Procedures associated with characterization via ^{1}H nuclear magnetic resonance (^{1}H NMR, Varian Inova 400 MHz spectrometer) spectroscopy, size exclusion chromatography (SEC, Viscotek GPC-Max), and small-angle X-ray scattering (SAXS, Rigaku S-Max 3000) have been described previously by our group.[26] Specific details associated with the application of these methods to this work have been included in the Supporting Information.

Rheology. Rheological melt experiments were run on a TA Instruments Advanced Rheometric Expansion System (ARES) rheometer. Dynamic temperature ramp tests were performed on dry polymer disks while heating and cooling at 1 °C min^{-1} at angular frequency of 1 rad s^{-1} and a strain of 7% (within the linear viscoelastic regime, determined by dynamic strain sweep experiments for each sample).[19] Rheological frequency sweeps (ω = 0.1−100 rad s^{-1}, γ = 7%, $\dot{\gamma}$ = 2% s^{-1}) performed on micelle solutions and swollen hydrogels were run at room temperature by using a lower tool "cup bath" base and an 8 mm stainless steel upper parallel plate. Nonphotocoupled solutions were placed in a small mass upon the center of the base, and photocoupled and swollen hydrogels were blotted and placed in the center of the base. For both samples, a constant force of approximately 5−10% compression was applied before any testing to ensure sufficient contact and prevent slip.

Mechanical Testing. Tensile tests were performed on rectangular hydrogel samples as described previously by our group.[26] Specific details associated with the application of these methods to this work have been included in the Supporting Information.

Cryo-TEM. Cryo-transmission electron microscopy (cryo-TEM, Tecnai Sphera microscope) was performed at the Technical University of Eindhoven by using previously published methods.[52] Specific details associated with the application of these methods to this work have been included in the Supporting Information. SO-anth and SO-OH samples were prepared as micelle dispersions in DI water at concentrations of 1 and 2 mg/mL, respectively. Micelles were obtained from the dispersal of SO-anth and SO solids prepared from melt-processed powders quenched in liquid nitrogen from 70 °C.

https://dx.doi.org/10.1021/acsapm.0c00108
ACS Appl. Polym. Mater. 2020, 2, 5377−5387

Determination of Changes in Q. Solutions of particular water to polymer mass ratio $Q_{initial}$ were photocoupled in rectangular mold to attain solid-like hydrogel properties. They were then swollen to equilibrium in DI water, achieving a new water to polymer ratio of Q_{final}. These two swollen states are compared in the article. To determine Q_{final}, measurements of initial and final dimensions were found by using a caliper and then used to calculate the corresponding volumes. In this way, the increase in volume is attributed to water imbibed after photocuring and placement in water as opposed to gravimetric measurements which do not take into account air bubbles in the dry polymer. Summing this increase in mass with the mass of water initially in the solution, a Q_{final} was determined.

DLS. Dynamic light scattering measurements were performed by using a ZEN3600 Zetasizer Nano particle analyzer. Measurements were taken on the solutions diluted to Q = 1000 g of water per g of polymer and performed at 25 °C, 173° detector angle, and a 4 mW 633 nm laser. All reported particle sizes and PDIs are based on the *Z*-averaged diameter determined by Zetasizer DLS measurement software.

■ ASSOCIATED CONTENT

Supporting Information

The Supporting Information is available free of charge at https://pubs.acs.org/doi/10.1021/acsapm.0c00108.

Experimental details are provided regarding methodology and materials; ^{1}H NMR and SEC, rheological temperature ramps, SAXS characterization data, dynamic frequency sweeps of annealed samples, DLS data, and swelling data are all presented comparing SO-OH and SO-anth systems; a table detailing the number of replicates used in each experiment (PDF)

■ AUTHOR INFORMATION

Corresponding Author

Travis S. Bailey − *Department of Chemical and Biological Engineering and School of Advanced Materials Discovery, Colorado State University, Fort Collins, Colorado 80523, United States;* orcid.org/0000-0001-7616-9142; Email: travis.bailey@colostate.edu

Authors

Nabila A. Huq − *Department of Chemical and Biological Engineering, Colorado State University, Fort Collins, Colorado 80523, United States;* orcid.org/0000-0001-5088-9758

René P. M. Lafleur − *Institute for Complex Molecular Systems, Eindhoven University of Technology, 5600 MB Eindhoven, The Netherlands;* orcid.org/0000-0003-0026-3428

Complete contact information is available at: https://pubs.acs.org/10.1021/acsapm.0c00108

Funding

This work was supported by the National Science Foundation under Grants CBET-1160026 and DMR-1808824, The Netherlands Organisation for Scientific Research (NWO Graduate Program 2010:022.002.028), and the Dutch Ministry of Education, Culture and Science (Gravity program 024.001.035). N.A.H. was also partially supported through the Walter Scott College of Engineering Graduate Teaching Fellowship Program at Colorado State University.

Notes

The authors declare no competing financial interest.

■ ACKNOWLEDGMENTS

The authors thank E. W. Meijer for his generous support of T.S.B. as a visiting professor in the Institute for Complex Molecular Systems at the Technical University of Eindhoven. They also thank Kathleen E. Berg and Dr. Charles S. Henry for providing access to the OmniCure Series 2000 UV light source as well as Kristine M. Fischenich for help photographing the hydrogel materials.

■ REFERENCES

(1) Annaka, M.; Matsuura, T.; Kasai, M.; Nakahira, T.; Hara, Y.; Okano, T. Preparation of Comb-Type N-Isopropylacrylamide Hydrogel Beads and Their Application for Size-Selective Separation Media. *Biomacromolecules* **2003**, *4* (2), 395−403.

(2) Susanto, H.; Ulbricht, M. Photografted Thin Polymer Hydrogel Layers on PES Ultrafiltration Membranes: Characterization, Stability, and Influence on Separation Performance. *Langmuir* **2007**, *23* (14), 7818−7830.

(3) Peppas, N. A.; Bures, P.; Leobandung, W.; Ichikawa, H. Hydrogels in pharmaceutical formulations. *Eur. J. Pharm. Biopharm.* **2000**, *50* (1), 27−46.

(4) Gong, C.; Shi, S.; Wang, X.; Wang, Y.; Fu, S.; Dong, P.; Chen, L.; Zhao, X.; Wei, Y.; Qian, Z. Novel Composite Drug Delivery System for Honokiol Delivery: Self-Assembled Poly(ethylene glycol)−Poly(ε-caprolactone)−Poly(ethylene glycol) Micelles in Thermosensitive Poly(ethylene glycol)−Poly(ε-caprolactone)−Poly(ethylene glycol) Hydrogel. *J. Phys. Chem. B* **2009**, *113* (30), 10183−10188.

(5) Dai, H.; Chen, Q.; Qin, H.; Guan, Y.; Shen, D.; Hua, Y.; Tang, Y.; Xu, J. A Temperature-Responsive Copolymer Hydrogel in Controlled Drug Delivery. *Macromolecules* **2006**, *39* (19), 6584−6589.

(6) Madaghiele, M.; Demitri, C.; Sannino, A.; Ambrosio, L. Polymeric hydrogels for burn wound care: Advanced skin wound dressings and regenerative templates. *Burns & trauma* **2014**, *2* (4), 153−61.

(7) Desai, P. N.; Yuan, Q.; Yang, H. Synthesis and Characterization of Photocurable Polyamidoamine Dendrimer Hydrogels as a Versatile Platform for Tissue Engineering and Drug Delivery. *Biomacromolecules* **2010**, *11* (3), 666−673.

(8) Hou, Y.; Schoener, C. A.; Regan, K. R.; Munoz-Pinto, D.; Hahn, M. S.; Grunlan, M. A. Photo-Cross-Linked PDMSstar-PEG Hydrogels: Synthesis, Characterization, and Potential Application for Tissue Engineering Scaffolds. *Biomacromolecules* **2010**, *11* (3), 648−656.

(9) Stile, R. A.; Burghardt, W. R.; Healy, K. E. Synthesis and Characterization of Injectable Poly(N-isopropylacrylamide)-Based Hydrogels That Support Tissue Formation in Vitro. *Macromolecules* **1999**, *32* (22), 7370−7379.

(10) Möller, S.; Weisser, J.; Bischoff, S.; Schnabelrauch, M. Dextran and hyaluronan methacrylate based hydrogels as matrices for soft tissue reconstruction. *Biomol. Eng.* **2007**, *24* (5), 496−504.

(11) Ho, E.; Lowman, A.; Marcolongo, M. Synthesis and characterization of an injectable hydrogel with tunable mechanical properties for soft tissue repair. *Biomacromolecules* **2006**, *7* (11), 3223−3228.

(12) Sannino, A.; Demitri, C.; Madaghiele, M. Biodegradable Cellulose-based Hydrogels: Design and Applications. *Materials* **2009**, *2* (2), 353−373.

(13) Parente, M. E.; Andrade, A. O.; Ares, G.; Russo, F.; Jimenez-Kairuz, A. Bioadhesive hydrogels for cosmetic applications. *Int. J. Cosmet. Sci.* **2015**, *37* (5), 511−518.

(14) Beziau, A.; Fortney, A.; Fu, L.; Nishiura, C.; Wang, H.; Cuthbert, J.; Gottlieb, E.; Balazs, A. C.; Kowalewski, T.; Matyjaszewski, K. Photoactivated Structurally Tailored and Engineered Macromolecular (STEM) gels as precursors for materials with spatially differentiated mechanical properties. *Polymer* **2017**, *126*, 224−230.

(15) Gohy, J.-F.; Zhao, Y. Photo-responsive block copolymer micelles: design and behavior. *Chem. Soc. Rev.* **2013**, *42* (17), 7117−7129.
(16) Guo, C.; Bailey, T. S. Highly distensible nanostructured elastic hydrogels from AB diblock and ABA triblock copolymer melt blends. *Soft Matter* **2010**, *6* (19), 4807−4818.
(17) Guo, C.; Bailey, T. S. Tailoring mechanical response through coronal layer overlap in tethered micelle hydrogel networks. *Soft Matter* **2015**, *11* (37), 7345−7355.
(18) Guo, C.; Lewis, J. T.; Scalfani, V. F.; Schwartz, M. M.; Bailey, T. S. Dangling-End Double Networks: Tapping Hidden Toughness in Highly Swollen Thermoplastic Elastomer Hydrogels. *Chem. Mater.* **2016**, *28* (6), 1678−1690.
(19) Huq, N. A.; Ekblad, J. R.; Leonard, A. T.; Scalfani, V. F.; Bailey, T. S. Phototunable Thermoplastic Elastomer Hydrogel Networks. *Macromolecules* **2017**, *50* (4), 1331−1341.
(20) May, A. W.; Shi, Z.; Wijayasekara, D. B.; Gin, D. L.; Bailey, T. S. Self-assembly of highly asymmetric, poly(ionic liquid)-rich diblock copolymers and the effects of simple structural modification on phase behaviour. *Polym. Chem.* **2019**, *10* (6), 751−765.
(21) Bates, F. S.; Fredrickson, G. H. Block Copolymers: Designer Soft Materials. *Phys. Today* **1999**, *52*, 32−38.
(22) Fischenich, K. M.; Boncella, K.; Lewis, J. T.; Bailey, T. S.; Haut Donahue, T. L. Dynamic compression of human and ovine meniscal tissue compared with a potential thermoplastic elastomer hydrogel replacement. *J. Biomed. Mater. Res., Part A* **2017**, *105* (10), 2722−2728.
(23) Fischenich, K. M.; Lewis, J. T.; Bailey, T. S.; Haut Donahue, T. L. Mechanical viability of a thermoplastic elastomer hydrogel as a soft tissue replacement material. *Journal of the Mechanical Behavior of Biomedical Materials* **2018**, *79*, 341−347.
(24) Lewis, J. T.; Fischenich, K. M.; Haut Donahue, T. L.; Bailey, T. S. Nanostructure-Driven Replication of Soft Tissue Biomechanics in a Thermoplastic Elastomer Hydrogel. *ACS Biomater. Sci. Eng.* **2018**, *4* (11), 3854−3863.
(25) Fischenich, K. M.; Pauly, H. M.; Lewis, J. T.; Bailey, T. S.; Haut Donahue, T. L. A Hydrogel Meniscal Replacement: Knee Joint Pressure and Distribution in an Ovine Model Compared to Native Tissue. *Ann. Biomed. Eng.* **2018**, *46* (11), 1785−1796.
(26) Huq, N. A.; Bailey, T. S. Spatial Control of Mechanical Properties and Surface Topography in a Photoreactive Block Copolymer Hydrogel. *Macromolecules* **2018**, *51* (19), 7734−7744.
(27) Lewis, J. T. Engineering Effective Fibrocartilage Replacement Technologies Using Nanostructure-driven Replication of Soft Tiussue Biomechanics in Thermoplastic Elastomer Hydrogels. CSU Theses and Dissertations, Colorado State University, Fort Collins, CO, 2018.
(28) Wang, Q.; Liu, P.; Sun, Y.; Gong, T.; Zhu, M.; Sun, X.; Zhang, Z.; Duan, Y. Preparation and properties of biocompatible PS-PEG/calcium phosphate nanospheres. *Nanotoxicology* **2015**, *9* (2), 190−200.
(29) Zheng, L. L.; Vanchinathan, V.; Dalal, R.; Noolandi, J.; Waters, D. J.; Hartmann, L.; Cochran, J. R.; Frank, C. W.; Yu, C. Q.; Ta, C. N. Biocompatibility of poly(ethylene glycol) and poly(acrylic acid) interpenetrating network hydrogel by intrastromal implantation in rabbit cornea. *J. Biomed. Mater. Res., Part A* **2015**, *103* (10), 3157−65.
(30) Bernard, M.; Jubeli, E.; Pungente, M. D.; Yagoubi, N. Biocompatibility of polymer-based biomaterials and medical devices - regulations, in vitro screening and risk-management. *Biomater. Sci.* **2018**, *6* (8), 2025−2053.
(31) Bates, F. S. Polymer-Polymer Phase Behavior. *Science* **1991**, *251* (4996), 898−905.
(32) Bates, F. S.; Schulz, M. F.; Khandpur, A. K.; Forster, S.; Rosedale, J. H.; Almdal, K.; Mortensen, K. Fluctuations, Conformational Asymmetry and Block-Copolymer Phase-Behavior. *Faraday Discuss.* **1994**, *98*, 7−18.
(33) Cavicchi, K. A.; Lodge, T. P. Domain size equilibration in sphere-forming block copolymers. *J. Polym. Sci., Part B: Polym. Phys.* **2003**, *41* (7), 715−724.
(34) Telitel, S.; Blasco, E.; Bangert, L. D.; Schacher, F. H.; Goldmann, A. S.; Barner-Kowollik, C. Photo-reversible bonding and cleavage of block copolymers. *Polym. Chem.* **2017**, *8* (27), 4038−4042.
(35) Scalfani, V. F. Part I — Access to UV Photocured Nanostructures via Selective Morphological Trapping of Block Copolymer Melts. Part II — Morphological Phase Behavior of Poly(RTIL) Containing Block Copolymer Melts. Ph.D. Dissertation, Colorado State University, Fort Collins, CO, 2012.
(36) Scalfani, V. F.; Bailey, T. S. Access to Nanostructured Hydrogel Networks through Photocured Body-Centered Cubic Block Copolymer Melts. *Macromolecules* **2011**, *44* (16), 6557−6567.
(37) Scalfani, V. F.; Wiesenauer, E. F.; Ekblad, J. R.; Edwards, J. P.; Gin, D. L.; Bailey, T. S. Morphological Phase Behavior of Poly(RTIL)-Containing Diblock Copolymer Melts. *Macromolecules* **2012**, *45* (10), 4262−4276.
(38) Shi, Z.; May, A. W.; Kohno, Y.; Bailey, T. S.; Gin, D. L. Metal-containing ionic liquid-based, uncharged-charged diblock copolymers that form ordered, phase-separated microstructures and reversibly coordinate small protic molecules. *J. Polym. Sci., Part A: Polym. Chem.* **2017**, *55*, 2961.
(39) Shi, Z.; Newell, B. S.; Bailey, T. S.; Gin, D. L. Ordered, Microphase-Separated, Noncharged-Charged Diblock Copolymers via the Sequential ATRP of Styrene and Styrenic Imidazolium Monomers. *Polymer* **2014**, *55* (26), 6664−6671.
(40) Bailey, T. S. Morphological behavior spanning the symmetric AB and ABC block copolymer states. Ph.D. Dissertation, University of Minnesota, Minneapolis, MN, 2001.
(41) Kossuth, M. B.; Morse, D. C.; Bates, F. S. Viscoelastic behavior of cubic phases in block copolymer melts. *J. Rheol.* **1999**, *43* (1), 167−196.
(42) Vigild, M. E.; Chu, C.; Sugiyama, M.; Chaffin, K. A.; Bates, F. S. Influence of Shear on the Alignment of a Lamellae-Forming Pentablock Copolymer. *Macromolecules* **2001**, *34* (4), 951−964.
(43) Cochran, E. W.; Bates, F. S. Shear-induced network-to-network transition in a block copolymer melt. *Phys. Rev. Lett.* **2004**, *93* (8), 087802.
(44) Krishnan, K.; Bates, F. S.; Lodge, T. P. Shear alignment of a swollen lamellar phase in a ternary polymer blend. *J. Rheol.* **2005**, *49* (6), 1395−1408.
(45) Wijayasekara, D. B.; Cowan, M. G.; Lewis, J. T.; Gin, D. L.; Noble, R. D.; Bailey, T. S. Elastic free-standing RTIL composite membranes for CO_2/N_2 separation based on sphere-forming triblock/diblock copolymer blends. *J. Membr. Sci.* **2016**, *511*, 170−179.
(46) Jain, S.; Bates, F. S. Consequences of nonergodicity in aqueous binary PEO-PB micellar dispersions. *Macromolecules* **2004**, *37* (4), 1511−1523.
(47) Scalfani, V. F.; Bailey, T. S. Thermally Stable Photocuring Chemistry for Selective Morphological Trapping in Block Copolymer Melt Systems. *Chem. Mater.* **2010**, *22* (21), 5992−6000.
(48) Egbe, D. A. M.; Turk, S.; Rathgeber, S.; Kuhnlenz, F.; Jadhav, R.; Wild, A.; Birckner, E.; Adam, G.; Pivrikas, A.; Cimrova, V.; Knor, G.; Sariciftci, N. S.; Hoppe, H. Anthracene Based Conjugated Polymers: Correlation between pi-pi-Stacking Ability, Photophysical Properties, Charge Carrier Mobility, and Photovoltaic Performance. *Macromolecules* **2010**, *43* (3), 1261−1269.
(49) Schwarz, F. P.; Wasik, S. P. Fluorescence Measurements of Benzene, Naphthalene, Anthracene, Pyrene, Fluoranthene, and Benzo[E]Pyrene in Water. *Anal. Chem.* **1976**, *48* (3), 524−528.
(50) Byron, C. M.; Werner, T. C. Experiments in Synchronous Fluorescence Spectroscopy for the Undergraduate Instrumental Chemistry Course. *J. Chem. Educ.* **1991**, *68* (5), 433−436.
(51) Fetters, L. J.; Lohse, D. J.; Richter, D.; Witten, T. A.; Zirkel, A. Connection between Polymer Molecular Weight, Density, Chain Dimensions, and Melt Viscoelastic Properties. *Macromolecules* **1994**, *27* (17), 4639−47.
(52) Wijnands, S. P. W.; Engelen, W.; Lafleur, R. P. M.; Meijer, E. W.; Merkx, M. Controlling protein activity by dynamic recruitment on a supramolecular polymer platform. *Nat. Commun.* **2018**, *9* (1), 65.

https://dx.doi.org/10.1021/acsapm.0c00108
ACS Appl. Polym. Mater. 2020, 2, 5377−5387

Supplementary Information for:

Melt-fabricated photoreactive block copolymer micelles as building blocks for tunable elastomeric hydrogels

*Nabila A. Huq[1], René P. M. Lafleur,[2] and Travis S. Bailey[1]**

[1] Department of Chemical and Biological Engineering, Colorado State University, Fort Collins, Colorado, 80521, USA

[2] Institute for Complex Molecular Systems, Eindhoven University of Technology, 5600 MB Eindhoven, The Netherlands

* Corresponding Author. *Email: travis.bailey@colostate.edu*

Table of Contents

1. Experimental Details

Materials

The materials associated with the syntheses of SO, SOS, and SO-*anth*, their purification prior to use, and general handling procedures have been described previously.[1, 2] Specific details from these references are reproduced here for convenience.

General. *Styrene (99%, 50 ppm p-tert-butylcatechol inhibitor, Aldrich) was purified by static vacuum (15-30 mTorr) distillations from di-n-butylmagnesium (1.0 M in heptane, Aldrich) at 40 °C. Ethylene oxide (flammable, toxic, 99.5+%, compressed gas, Aldrich) was purified by successive distillations (vacuum distillations can result in pressure explosions if care is not taken) from di-n-butylmagnesium (1.0 M in heptane, Aldrich) at 3 °C. sec-butyllithium (1.3 M in cyclohexane/hexane, Fisher) was used as received. Potassium naphthalenide solution was prepared according to a previous report.[3] 9-(chloromethyl)anthracene (98%, Aldrich) and α,ά-dibromo-p-xylene (97%, Aldrich) were dried under high vacuum for several hours prior to use. Tetrahydrofuran (THF) was degassed by sparging with argon (10 psi) for a period of 45 minutes and then purified over two molecular sieve columns of neutral alumina (Glass Contour, Inc.). Cyclohexane (CHX) was degassed with argon and purified through a column of neutral alumina followed by a column of Q5 copper (II) oxide catalyst (Glass Contour, Inc.). Hydrogels were swollen using DI water of 18.2 MΩ resistivity (Evoqua/U.S. Filter Service Deionization). Other common chemicals and solvents were used as received unless otherwise stated. Ultra-high purity argon (99.998% Airgas) was passed through a column of 5 Å molecular sieves with Drierite (Agilent) and oxygen absorbing purifier column (Matheson Tri-gas). Glassware and polymerization reactors were flamed under vacuum and backfilled with argon (3X).*

Instrumentation

Procedures associated with characterization via ^{1}H nuclear magnetic resonance (NMR, Varian Inova 400 MHz spectrometer) spectroscopy, size exclusion chromatography (SEC, Viscotek GPC-Max), Small Angle X-ray Scattering (SAXS, Rigaku S-Max 3000), tensile testing (TA ARES) and cryo-transmission electron microscopy (cryo-TEM, Tecnai Sphera microscope) have been described previously.[1, 4] Specific details from these references are reproduced here for convenience.

NMR*. ^{1}H NMR spectra were recorded at room temperature on a Varian Inova 400 MHz spectrometer with a d1 pulse delay of at least 20 s to ensure complete relaxation of end-groups. Spectra were referenced to $CDCl_3$ solvent.*

SEC. *Size exclusion chromatography (SEC) spectra were collected on a Viscotek GPC-Max chromatography system outfitted with three 7.5 x 340 mm Polypore™ (Polymer Laboratories) columns in series, a Viscotek differential refractive index (RI) detector, and an Alltech column oven (mobile phase DMF, 40 °C, 1 mL min^{-1}).*

SAXS. *Small Angle X-ray Scattering (SAXS) data were collected on a Rigaku S-Max 3000 High Brilliance three pinhole SAXS system outfitted with a MicroMax-007HFM rotating anode (CuKα), Confocal Max-Flux™ Optic, Gabriel multiwire area detector, and a Linkam thermal stage. Typical sample to detector distances were on the order of two meters resulting in a q range of approximately 0.006 to 0.18 Å^{-1}. Exposure times used resulted in no detectable sample degradation (SEC). Dry polymer samples were sandwiched between Kapton windows (0.05 – 0.5 mm thick X 10 mm diameter). Scan times were typically on the order of 3600 s, with temperature ramp rates of 10 °C min^{-1}.*

Mechanical Testing*. Tensile tests were performed on rectangular hydrogel samples at room temperature using the normal force transducer of a TA ARES rheometer. TA rectangular torsion geometry test fixtures modified with sandpaper were used as tensile test grips, and a strain rate of 2 % s^{-1} was applied until slip or fracture. Engineering stress was calculated using sample cross-sectional area-normalized force.*

Cryo-TEM. *Micelle dispersions in DI water (1 mg/mL and 2 mg/mL) were vitrified using a computer-controlled vitrification robot (FEI Vitrobot™ Mark III, FEI Company). Lacey carbon films on 200 mesh copper grids (LC200-CU, Electron Microscopy Sciences) were surface plasma treated with a Cressington 208 carbon coater. Vitrified films were transferred into the vacuum of a Tecnai Sphera microscope with a Gatan 626 cryoholder. The microscope is equipped with an LaB_6 filament that was operated at 200 kV, and a bottom mounted 1024x1024*

Gatan charged-coupled device (CCD) camera. The Vitrobot was operated at 22 °C and at a relative humidity of 100%. In the preparation chamber of the 'Vitrobot', a 3µl sample was applied on a Lacey carbon film which was surface plasma treated for 40 s at 5 mA just prior to use. Excess sample was removed by blotting using two filter papers for 3 s at –3 mm, and the thin film thus formed was plunged (acceleration about 3 g) into liquid ethane just above its freezing point. The vitrified films were observed in the Tecnai Sphera microscope at temperatures below -170 °C. Micrographs were taken at low dose conditions, at a magnification of 25000 and at -5 µm defocus.

2. ^{1}H-NMR spectrum and GPC traces of SO-anth and precursors.

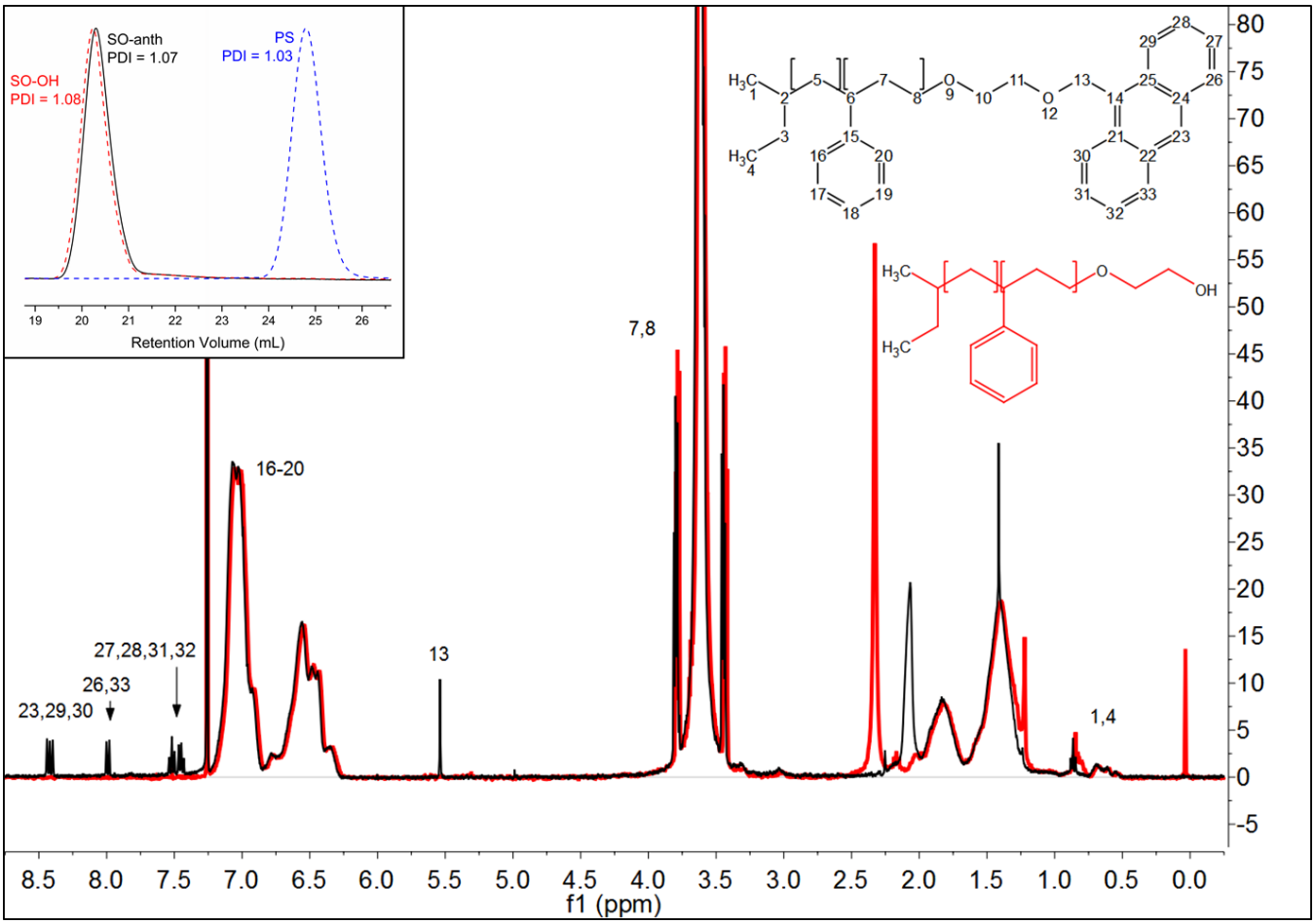

Figure S1. Overlaid SO-OH and SO-anth ^{1}H-NMR (with peak assignments) and SEC traces (inset) showing nearly identical molecular weight distributions.

^{1}H NMR Details:[2, 3, 5] (400 MHz, $CDCl_3$, δ): 8.4–8.5 (m, anthracene H_1, H_8 and H_{10}), 7.9–8.0 (d, anthracene H_4 and H_5), 7.4–7.6 (m, anthracene H_2, H_3, H_6 and H_7), 6.2–7.2 (b, –CH_2–C(R)H–C_6H_5), 5.5 (s, –O–CH_2–anthracene), 3.4–3.8 (b, –CH_2–CH_2–O–), 1.1–2.3 (b, –CH_2–C(R)H–C_6H_5), 0.8–0.9 (b, CH_3–CH_2–C(R)H–CH_3), 0.5–0.7 (b, CH_3–CH_2–C(R)H–CH_3).

3. Comparison of SO-anth and SO-OH melt-state self-assembly data

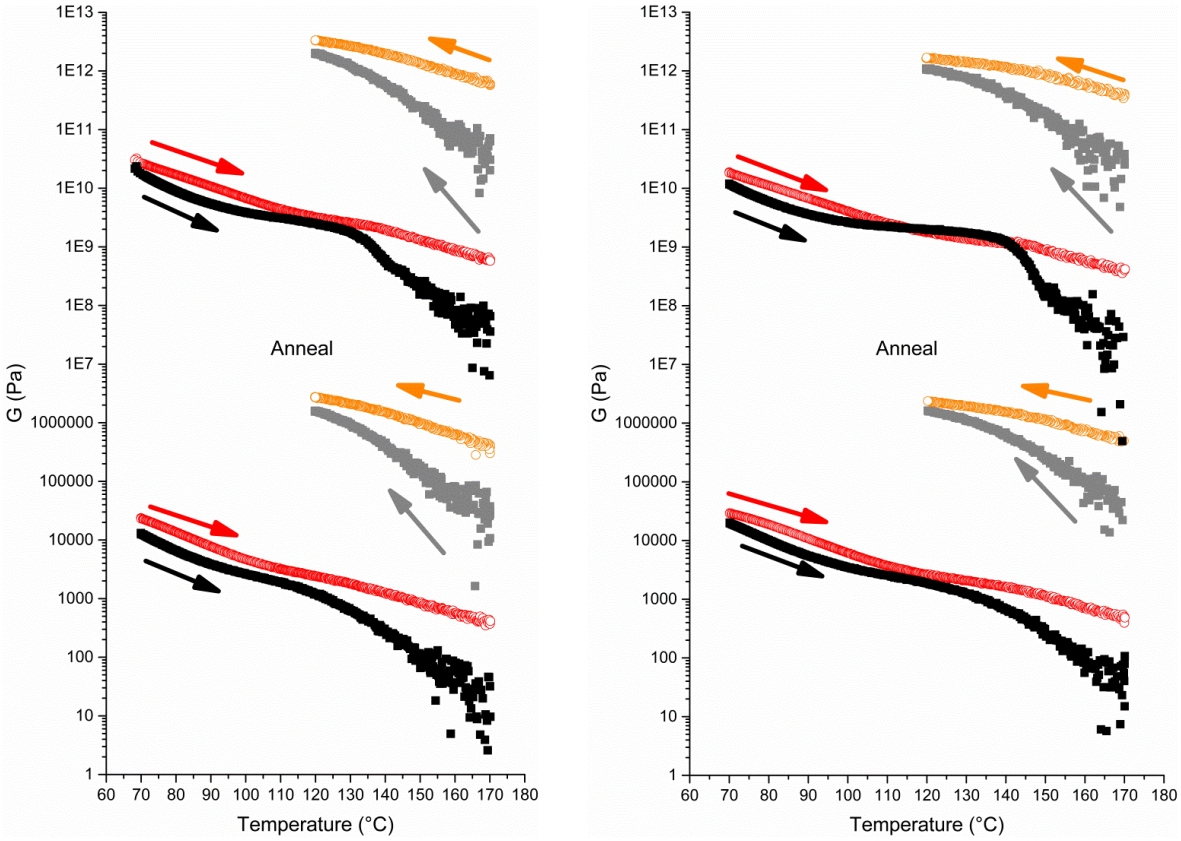

Figure S2. A series of consecutive rheological temperature ramp measurements (1 °C min^{-1}, ϵ = 1 %, ω = 1 Hz) performed on SO-anth (left) and SO-OH (right). Experiments were performed as follows (plotted from low to high): Samples were initially heated from 70 ˚C to 170 ˚C, cooled to 120 ˚C, annealed in situ for 4 hours and slowly cooled to 70 ˚C (not shown), heated through a second cycle from 70 ˚C to 170 ˚C, and then cooled back to 120 ˚C once more. The experiments demonstrate that both SO-OH and SO-anth samples gain an increase in modulus from annealing, associated with organization of the BCC lattice of micelles over time. However, heating past the transition (inflection in G') that is produced post-annealing around 140 ˚C results in complete loss of the higher order state gained during annealing. We believe this transition reflects a disordering transition from BCC to LLP of micelles. Solid circles indicate storage moduli data (G') and open circles are loss moduli data (G").

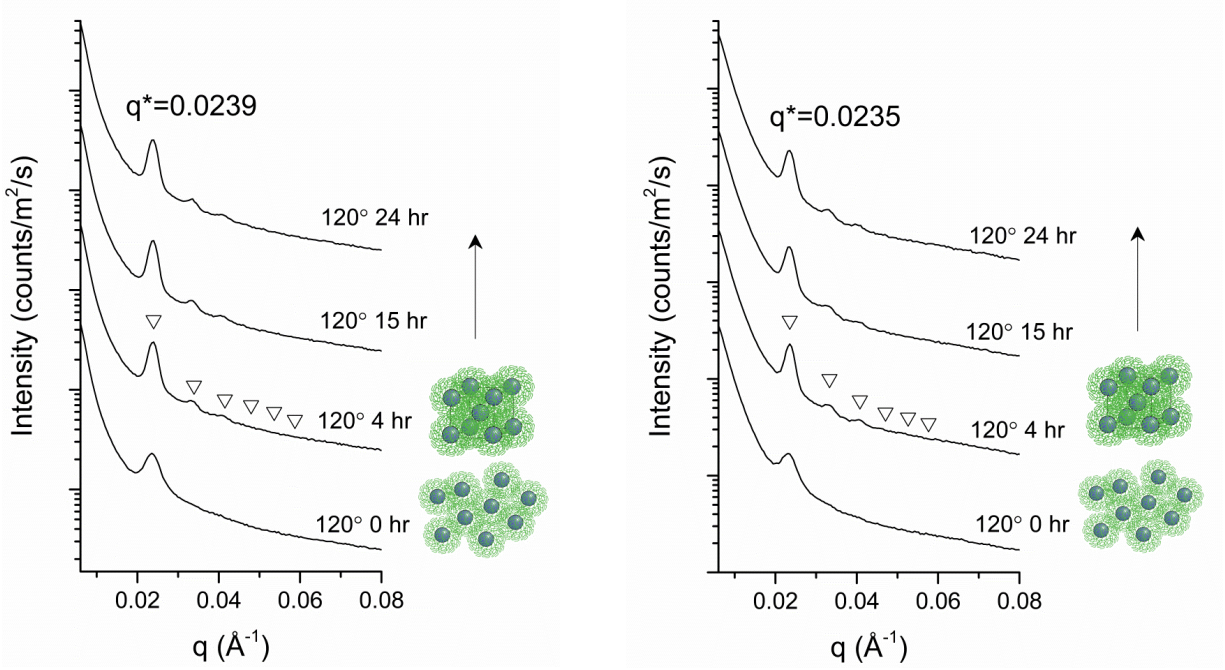

Figure S3. SAXS annealing (120 °C) of SO-anth (left) and SO-OH (right), showing adoption of a BCC lattice in the sphere morphology of micelles beginning at four hours.

Table S1. Micelle structural characterization information based on SAXS data.

Sample	f_{PS} [a]	q*/Å^{-1} [b]	d_{110}/nm [c]	a_{BCC}/nm [d]	R[a]/nm [e]	θ_{PS} [f]	$M_n/10^6$ g mol^{-1} [g]
SO-Anth (nh3-19)	0.122	0.0239	26.3	37.2	9.0	221	16.3
SO-OH (nh2-207)	0.125	0.0235	26.7	37.8	9.2	232	17.1

[a]Polystrene volume fraction, [b]primary scattering peak, [c]d-spacing for 110 crystal plane, [d]unit cell lattice constant [e]apparent radius, [f]mean aggregation number (i.e., PS chains per sphere), [g]estimated molecular weight of micelle.

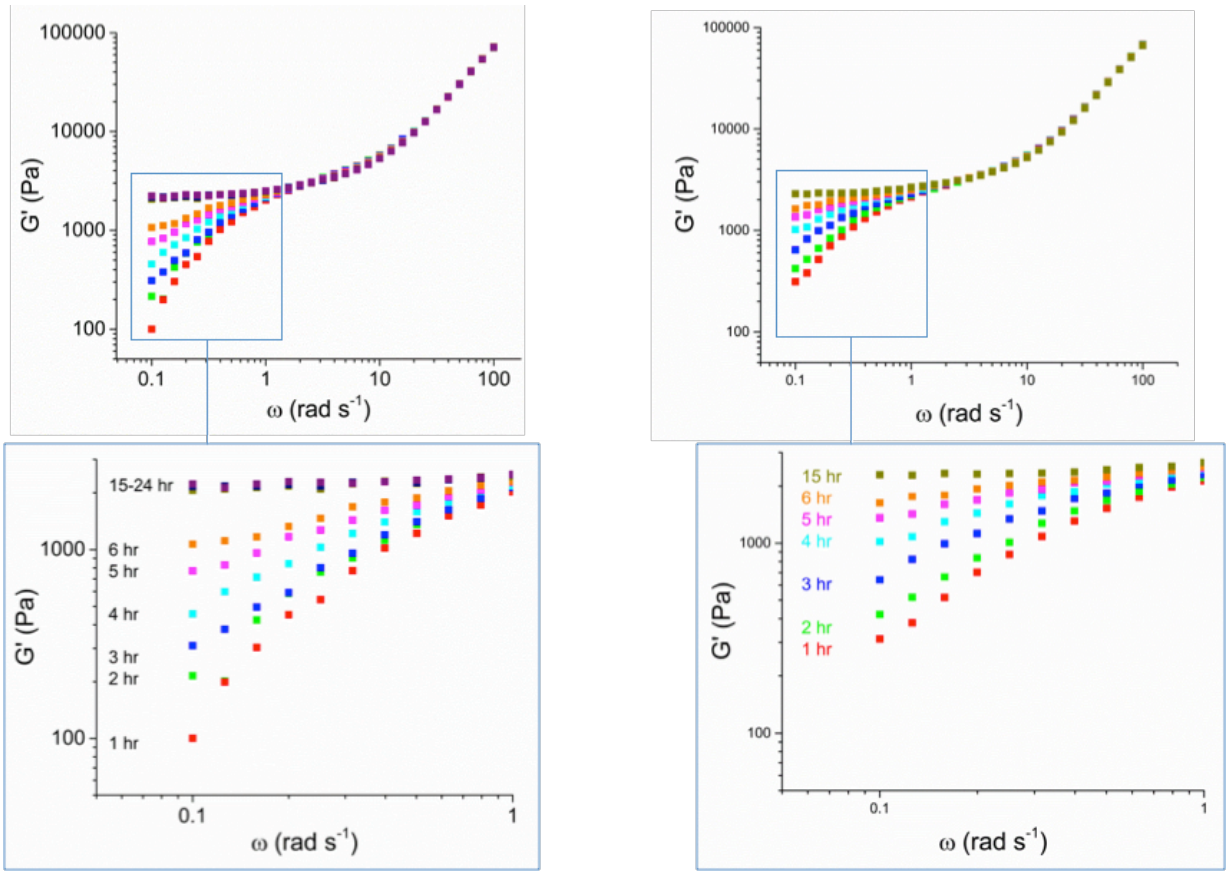

Figure S4. Rheological frequency sweeps under oscillatory shear at 120 °C (ω = 1 rad s^{-1}, γ = 7%) for both SO-anth (left) and SO-OH (right), with log G' plotted vs. log ω. Data shows the progression from liquid-like terminal relaxation behavior at a slope of ~2 to a highly ordered BCC lattice with a frequency independent plateau (0 slope) over the course of 15 hours.

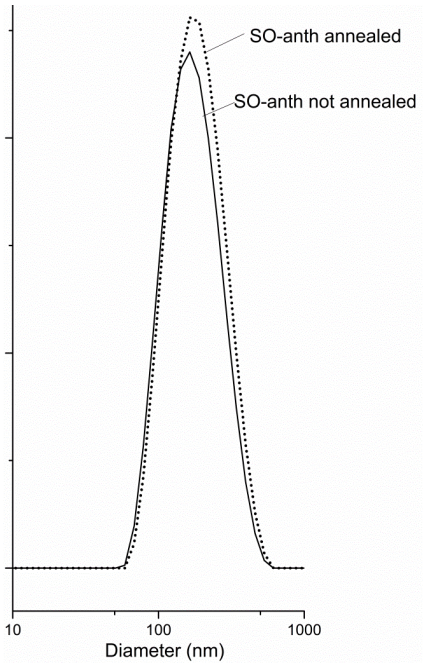

Figure S5: Comparison of hydrated SO-anth micelles produced with four hours annealing (BCC) versus those produced without annealing (5 minute melt press only).

4. Examination of SO-anth and SO-OH building block architecture in solution

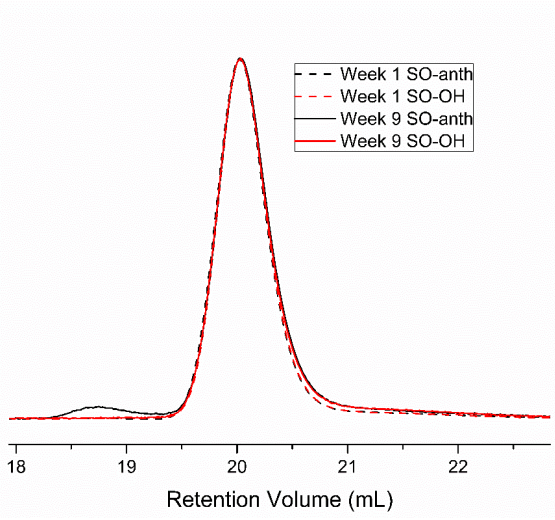

Figure S6. Overlaid GPC traces of SO-anth and SO-OH polymer species taken from micelles persisting in solutions for one and nine weeks. Traces show no change in molecular weight distribution over time save a small amount of SO-anth photocoupling to form SOS in the 9-week old SO anth micelles.

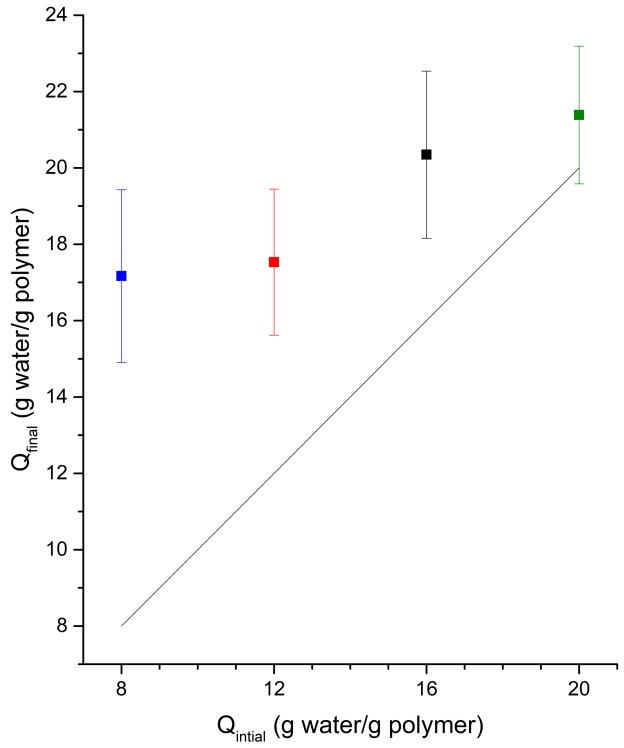

Figure S7. Solutions of $Q_{initial}$ = 8, 12, 16, and 20 g water per g polymer were irradiated for 5 min and swelled to their equilibrium state at Q_{final}. Values of Q_{final} were only moderately positively correlated with $Q_{initial}$ solution concentrations, each solution appearing to approach a mean final value between 18 and 21, with ΔQ diminishing with increasing $Q_{initial}$ (minimal additional swelling occurring after photocoupling at $Q_{initial}$ = 20). The line for no swelling is shown for reference.

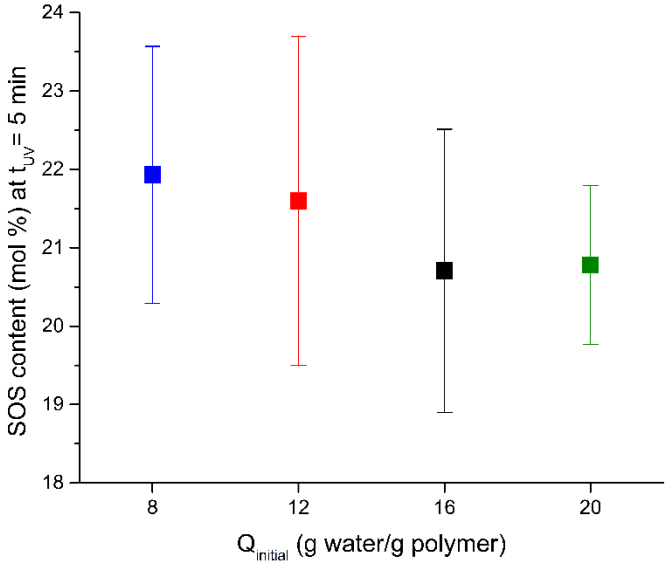

Figure S8. SOS triblock copolymer content (mol%, mean with a standard deviation of error shown) had a small, negative correlation with $Q_{initial}$, showing minimal influence of solution concentration on degree of tethering achievable after 5 min of UV irradiation.

5. Number of Trials per Experiment

Table S2.

# Trials	$Q_{initial}$				t_{UV}			
	8	**12**	**16**	**20**	**0**	**2.5**	**5**	**7.5**
G'	8	9	7	8	2	3	3	3
SOS	4	4	4	3	3	3	3	3
Q (SI)	7	7	7	8				
Tensile	2	3	2	2				

6. Sample Identification History

Table S3.

Manuscript ID	**Lab Notebook ID**
S-OH	DBW1142
SO-OH	NH2207
SO-anth	NH3012/NH3019/NH4053

7. References

1. Huq, N. A.; Bailey, T. S. Spatial Control of Mechanical Properties and Surface Topography in a Photoreactive Block Copolymer Hydrogel. *Macromolecules* **2018,** 51, (19), 7734-7744.

2. Huq, N. A.; Ekblad, J. R.; Leonard, A. T.; Scalfani, V. F.; Bailey, T. S. Phototunable Thermoplastic Elastomer Hydrogel Networks. *Macromolecules* **2017,** 50, (4), 1331 - 1341.

3. Guo, C.; Bailey, T. S. Highly Distensible Nanostructured Elastic Hydrogels from AB Diblock and ABA Triblock Copolymer Melt Blends. *Soft Matter* **2010,** 6, (19), 4807-4818.

4. Wijnands, S. P. W.; Engelen, W.; Lafleur, R. P. M.; Meijer, E. W.; Merkx, M. Controlling protein activity by dynamic recruitment on a supramolecular polymer platform. *Nat Commun* **2018,** 9, (1), 65.

5. Coursan, M.; Desvergne, J. P.; Deffieux, A. Reversible photodimerisation of ω-anthrylpolystyrenes. *Macromolecular Chemistry and Physics* **1996,** 197, (5), 1599-1608.